Molecular Origins of Homogeneous Crystal Nucleation

Peng Yi[1] and Gregory C. Rutledge[2]

[1]Department of Physics and [2]Department of Chemical Engineering, Massachusetts Institute of Technology, Cambridge, Massachusetts 02139; email: pengyi@mit.edu, rutledge@mit.edu

Annu. Rev. Chem. Biomol. Eng. 2012. 3:157–82

First published online as a Review in Advance on March 9, 2012

The *Annual Review of Chemical and Biomolecular Engineering* is online at chembioeng.annualreviews.org

This article's doi:
10.1146/annurev-chembioeng-062011-081029

1947-5438/12/0715-0157$20.00

Keywords

molecular simulation, order parameter, reaction coordinate, Ising model, Lennard-Jones, *n*-alkane

Abstract

We review the molecular principles underlying the homogeneous nucleation of a crystal phase from the melt phase, as elucidated by molecular simulation methods. Classical nucleation theory serves as the starting point for describing the nature of nucleation processes, but it does not derive from molecular principles itself. Density functional theory and molecular simulations offer tools for delving into the molecular origins of nucleation. Here, we emphasize the rapid development of molecular simulation methodologies for studying crystal nucleation from the melt. These methodologies are broadly categorized as free energy sampling methods, dynamical or mean first-passage time methods, and composite approaches that take advantage of both. The crucial selection of order parameters to distinguish the crystal phase from the liquid phase and important features of the reaction coordinate are emphasized. The system size dependence of the nucleation free energy barrier is also examined.

INTRODUCTION

Nucleation is a process that governs a broad spectrum of physicochemical phenomena. Among the different types of nucleation, homogeneous nucleation refers to the creation of a new phase in the absence of foreign agents or surfaces. Nucleation often is facilitated by the action of foreign substances or surfaces, which results in what is commonly called heterogeneous nucleation. Although the conditions required to realize homogeneous nucleation in real systems can often be quite difficult to achieve, the concepts and principles of homogeneous nucleation are the simplest and form the starting point for analyzing other types of nucleation. Numerous textbooks and reviews have covered the theoretical formulation of nucleation processes, e.g., Zettlemoyer (1), Skripov (2), Oxtoby (3), Debenedetti (4) and Kashchiev (5).

Early studies of nucleation began with the liquid-vapor phase transition (i.e., vapor condensation or liquid boiling) but were soon extended to the crystal-liquid phase transition. The latter is somewhat more complex owing to the change of symmetry that takes place upon passing from a liquid phase to a crystal phase. Transitions between liquid and vapor phases can be continuous owing to the existence of the critical point, but transitions between liquid and solid phases are generally first order. In addition, the experimental observation of crystallization from solution or melt is complicated by the fact that it occurs within the interior of a dense liquid. Therefore, the molecular origins and microscopic mechanism of homogeneous crystal nucleation remain poorly understood. With the development of computer technology, numerical simulation has become a useful tool in the study of homogeneous nucleation in the past 20 years, during which time new concepts and methods have been developed. This chapter reviews the development of simulation methods for the study of homogeneous nucleation, in particular that of crystal nucleation from a dense liquid. To give a complete description, a brief recap of the basic theories and common experimental methods is also presented.

Although the focus here is homogeneous crystal nucleation from a single-component melt, many interesting and closely related topics are also worth mentioning. A short list of these includes homogeneous nucleation from solution (6), binary homogeneous nucleation, heterogeneous crystal nucleation (7), crystal nucleation induced by external fields, nucleation under confinement, crossover of homogeneous nucleation to spinodal decomposition, and homogeneous nucleation in glasses. These topics also draw significant interest from both academia and industry.

NUCLEATION THEORIES

Classical Nucleation Theory

Classical nucleation theory (CNT) (8) has been widely applied to study homogeneous nucleation. Gibbs (9), Volmer & Weber (10), Becker & Döring (11), Zeldovich (12), and others first developed CNT to describe the condensation of a vapor to a liquid; this treatment was then extended to crystal nucleation from melts and solutions. In the thermodynamic formulation of CNT, a nucleus consisting of a thermodynamically more stable phase is separated from the surrounding, less stable phase by a sharp, infinitely thin interface. At state points displaced from the equilibrium thermodynamic phase transition point, e.g., by supersaturation, the competition between the free energy benefit associated with transforming the interior of the nucleus from the less stable phase to the more stable phase and the free energy required to create the interface between the two phases gives rise to a free energy barrier. For a spherical nucleus of radius r, the free energy of formation ΔG can be written as

$$\Delta G = 4\pi r^2 \sigma - \frac{4\pi r^3}{3} \Delta G_V , \qquad 1.$$

where σ is the interfacial free energy per unit area between phases, e.g., liquid and crystal, and ΔG_V is the Gibbs free energy difference per unit volume between the phases at the chosen state point. In most cases involving homogeneous crystal nucleation from the melt, one is concerned with displacement of the system from equilibrium by a reduction in temperature below the equilibrium melting temperature, which is called supercooling; our discussion of nucleation proceeds with this particular case in mind, but other types of driving forces for nucleation can be treated similarly. The top of the free energy barrier corresponds to the critical free energy ΔG^* required to form a critical nucleus of radius r^*. ΔG^* and r^* are obtained by maximizing ΔG with respect to r in Equation 1:

$$\Delta G^* \equiv \Delta G(r^*) = \frac{16\pi}{3}\frac{\sigma^3}{(\Delta G_V)^2}, \quad 2.$$

and

$$r^* = \frac{2\sigma}{\Delta G_V}. \quad 3.$$

Correspondingly, the size of the critical nucleus for the spherical nucleus model is

$$n^* = \rho_n \frac{4\pi r^{*3}}{3} = \frac{32\pi\rho_n}{3}\left(\frac{\sigma}{\Delta G_V}\right)^3, \quad 4.$$

where ρ_n is the molecule number density of the crystal phase. For clarity, we mention that some authors reserve the term "nucleus" for a molecular cluster of size equal to or greater than n^* and use the term "embryo" to refer to a molecular cluster of size smaller than n^*. The term "nucleation" then refers to the formation of one nucleus that serves as a stable center for further crystal growth. However, we do not make such a distinction here. All clusters, even those as small as one molecular unit, are equivalently referred to as nuclei, and the nuclei of size n^* are called critical nuclei.

For a small degree of supercooling $\Delta T/T_m$, ΔG_V can be approximated by

$$\Delta G_V \approx \rho_n \Delta H_f \Delta T / T_m, \quad 5.$$

where ΔH_f is the heat of fusion per molecule at the equilibrium melting temperature T_m, and ΔT (equal to $T_m - T$) is the supercooling. For deeper supercooling, a more accurate approximation is the following:

$$\Delta G_V \approx \rho_n \Delta H_f T\, \Delta T / T_m^2. \quad 6.$$

Using the first-order approximation of Equation 5, the temperature dependence of the critical nucleus size and the critical free energy is given by

$$r^* \propto (\Delta T)^{-1} \quad 7.$$

and

$$\Delta G^* \propto (\Delta T)^{-2}. \quad 8.$$

The kinetic approach to nucleation is based on the Szilard model (13), in which a nucleus changes size solely by the attachment and detachment of monomers. Stationary nucleation, in which the nucleation rate is time independent, is the simplest case of nucleation. During stationary nucleation, the nucleus size distribution remains unchanged until the monomer concentration in the system begins to decrease owing to depletion of monomers in favor of the growing nuclei. Detailed derivations can be found in many textbooks, e.g., Kashchiev (5). The rate of nucleation, i.e., the number of critical nuclei formed per unit time per unit volume, can be expressed in the form of the Arrhenius equation:

$$I = I_0 e^{-\Delta G^*/k_B T}, \quad 9.$$

where I_0 is a kinetic prefactor and k_B is the Boltzmann constant. I_0 is given by

$$I_0 = \rho_0 \nu, \qquad 10.$$

where ρ_0 is the molecule number density in the melt state, and ν is the frequency of molecular transport at the nucleus surface. Furthermore, ν is often approximated using the Stokes-Einstein relation

$$\nu \approx k_B T / 3\pi a_0^3 \eta, \qquad 11.$$

where a_0 is the molecular diameter and η is the viscosity (14).

In the liquid-vapor transition, the viscosity is not strongly temperature dependent; therefore, when the supercooling ΔT for the liquid-vapor transition increases, the nucleation rate increases exponentially according to Equations 8 and 9. However, in the solid-liquid transition, when the supercooling ΔT increases, not only does ΔG^* decrease, but also a sharp increase occurs in viscosity η, which restricts molecular movement and inhibits the formation of crystal structure. Turnbull & Fisher (15) quantified this behavior with a free energy barrier to diffusion. Therefore, in the case of crystal nucleation from a dense liquid, one can rewrite Equation 9 as follows:

$$I = A e^{-E_d/k_B T} e^{-\Delta G^*/k_B T} = A e^{-(E_d + \Delta G^*)/k_B T}, \qquad 12.$$

where A is a temperature-independent factor and E_d is the diffusion free energy barrier. As a result, as the supercooling increases, the nucleation rate reaches a maximum at a temperature T_{max} and subsequently decreases. T_{max} is normally intermediate between the melting point T_m and the glass transition temperature T_g.

The Arrhenius form of Equation 9 suggests that transition state theory (TST), which has been widely applied to evaluate the temperature dependences of chemical reaction rates, can be applied to study nucleation processes. According to TST, the transition from the reactant to the product during a chemical reaction occurs by passage through a transition state, and the energy needed for the reactants to reach the transition state is called the activation energy. TST is analogous to CNT, in which the metastable state is the reactant, the stable state is the product, and the two states are separated by the critical state, which corresponds to the transition state in the TST terminology. The activation energy in a nucleation event is the critical free energy.

Induction Time

The nucleation rate measures how frequently nucleation events occur. The higher the nucleation rate is, the faster a system escapes the metastable supercooled state. The ability of a system to sustain small thermal fluctuations while in a metastable equilibrium state is characterized by the induction time τ^*, which is defined as the time elapsed between the establishment of supercooling and the appearance of persistent, stable nuclei. The induction time is closely related to the nucleation rate, and the relation depends on whether the system escapes the metastable state by a mononuclear mechanism or a polynuclear mechanism (5).

The mononuclear mechanism of nucleation applies to systems that undergo phase transition through the appearance of exactly one stable nucleus. In this case, the induction time τ^* is related to the nucleation rate I by

$$\tau^* = \frac{1}{IV}, \qquad 13.$$

where V is the volume of the system. Through this relation, the nucleation rate can be calculated when τ^* and V are both known. By contrast, the polynuclear mechanism applies to systems that

undergo phase transition through the appearance of statistically multiple stable nuclei. In this case,

$$\tau^* = [(1 + vd)\alpha_d/(c_g G_c^{vd} I)]^{1/(1+vd)}, \quad 14.$$

where d is the dimensionality of the system; c_g is a shape factor whose magnitude is on the order of one; G_c is the crystal growth rate; v is the growth exponent, which is also on the order of one; and α_d is the detectable fraction of crystallized volume. A unified formula for the induction time, considering both mechanisms, is provided by Kashchiev (see equation 29.12 in Reference 5):

$$\tau^* = 1/IV + [(1 + vd)\alpha_d/(c_g G_c^{vd} I)]^{1/(1+vd)}. \quad 15.$$

When the system volume is large, Equation 15 reduces to Equation 14, the polynuclear case; when the system volume is small, Equation 15 reduces to Equation 13, the mononuclear case. According to Equation 15, the role of I is weaker in the polynuclear case than in the mononuclear case, and the induction time does not depend on the volume.

Experimentally, the detectable size of a nucleus is normally somewhat larger than the critical size, n^*. Therefore, depending on the resolution of the measurement techniques employed, e.g., visual measurement, light scattering, or electric sensing methods, some amount of crystal growth must take place between the critical nucleation event and its subsequent detection. However, the growth rate is normally so much faster than the nucleation rate that once the critical nucleation event occurs, the crystal grows to detectable size quite quickly, and the observed induction time differs only marginally from the true one. For this reason, induction time measurements remain the most reliable method for characterizing the kinetics of nucleation.

Equations 13–15 were derived on the assumption that the nucleation is stationary. In reality, the nucleation process cannot be stationary during the short transient period immediately following the imposition of supercooling, during which time the system reequilibrates to its new, metastable state. This transient gives rise to a time lag, τ', before the stationary nucleation condition is fulfilled. The observed induction time generally includes this time lag, so that Equation 13, for example, should be rewritten as

$$\tau^* = b\tau' + 1/IV, \quad 16.$$

where $b \approx 1$ is a numerical factor that depends on the details of nucleation during the transient period. The time lag is often proportional to the viscosity of the melt and can be as long as hours or days for viscous melts (5). When a system is highly viscous, τ' can be much greater than $1/IV$, and the induction time is then determined by τ'.

Density Functional Theory

One of the main criticisms of CNT is the capillary approximation: small portions of the new phase are treated as if they represent macroscopic domains. This approximation implies that material within the nucleus behaves like the new phase in bulk and that the interfacial free energy of the nucleus is the same as that between two macroscopic, bulk phases. These assumptions hold only when the nuclei are sufficiently large, which makes CNT most applicable for nucleation near the thermodynamic equilibrium, also known as the coexistence point. Farther away from coexistence, especially as the system approaches the spinodal, CNT could become very inaccurate. Compared with the nucleation rates obtained in experiments, the nucleation rates predicted by CNT, using independently measured thermodynamic properties such as interfacial free energies and heats of fusion of macroscopic phases, are generally several orders of magnitude too low at low temperatures, and too high at high temperatures. **Figure 1**, for example, shows the experimental and theoretical nucleation rates for liquid water from a supersaturated vapor. Under such

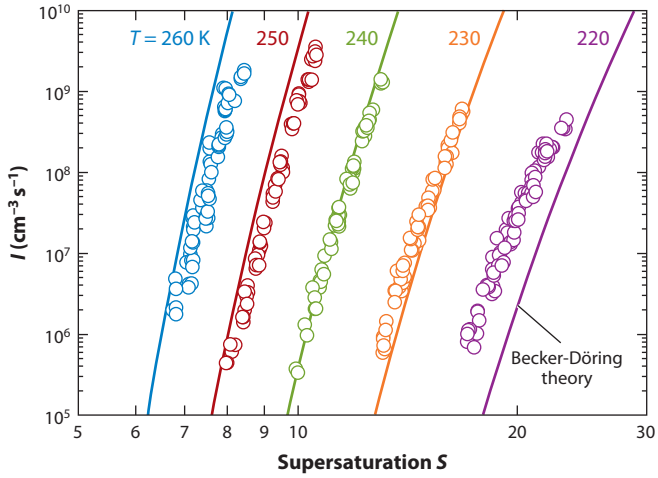

Figure 1

Nucleation rates in supersaturated H_2O vapor as a function of supersaturation S for various temperatures ranging from 220 to 260 K. Experimental measurements are denoted by open circles, whereas classical nucleation theory (Becker-Döring theory) predictions are denoted by lines. Reprinted with permission from Reference 16. Copyright © 2001 American Chemical Society.

circumstances, a more sophisticated, molecular approach is needed. Density functional theory (DFT) is one such approach and is discussed briefly below. Another molecular approach based on molecular simulation is then discussed in more detail.

DFT is a modeling method used in physics and chemistry to study many-body systems by using their density distributions to characterize the structures of the systems. DFT can be applied quantum mechanically, at the electronic level, as well as classically, at the scale of atoms and molecules. It has also proved to be a powerful approach to study nucleation of the vapor-liquid transition, as shown by Cahn & Hilliard (17), Abraham (18), and Oxtoby & Evans (19). In DFT, one expresses the free energy of a system as a functional of radial density profile $\rho(r)$. The density varies from the center of the nucleus outward. The density at the center of the nucleus does not have to be the same as that of the bulk new phase, nor does the change in density in the vicinity of the locus where the inner and outer phases meet have to mimic that of the interface between macroscopic phases.

For vapor-liquid nucleation, Oxtoby (20) has shown that DFT yields more accurate results than CNT. DFT calculations for Lennard-Jones fluids have shown that effects not captured by CNT are much more pronounced in bubble nucleation than in droplet nucleation (21). DFT was also applied to *n*-alkanes, where it was found that there is a clear effect of chain length on nucleation behavior (22). For binary condensation, Oxtoby & Kashchiev (23) offered a thermodynamic proof of the nucleation theorem (24) and extended its applicability to multicomponent homogeneous nucleation. According to the nucleation theorem, the critical free energy, the free energy of phase change (e.g., fusion), and the critical nucleus size are related by

$$\frac{\mathrm{d}\Delta G^*}{\mathrm{d}\Delta G_V} = -n^*. \qquad 17.$$

Equation 17 holds true regardless of the particular definition of a nucleus, and it provides the possibility of optimizing the nucleus size definition even at the microscopic level.

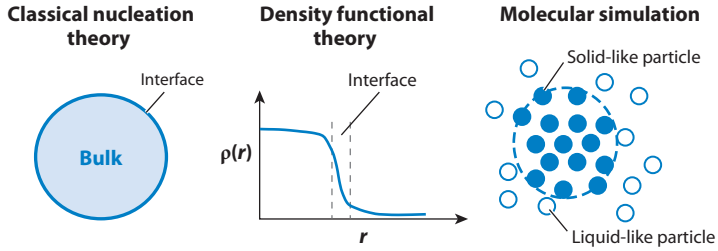

Figure 2

Three approaches to the nucleation problem and the representation of the nucleus in each approach.

Harrowell & Oxtoby (25) extended application of the DFT method to the solid-liquid transition. Because a solid-liquid transition involves not only a density change but also a change in structural order, the free energy was taken to be a functional of not only the density profile but also the Fourier components of the lattice structure (26). They observed that the interface tends to be much sharper for the solid nucleating within the melt under supercooled conditions than for the melt nucleating within the solid under superheated conditions; the solid-liquid interfacial free energy was calculated to be consistent with other methods (26). These investigators observed that the properties of the critical nucleus can differ significantly from those of the stable bulk phase that eventually forms. They have applied this method to the study of protein crystallization from aqueous solution (27), in which protein concentration and crystal structure evolve together but not necessarily at the same rate. Application of the density functional approach to these situations should yield more information on these systems and resolve many other problems inherent in the CNT.

Molecular simulation comprises a group of methods that are suitable for the study of nucleation involving critical nuclei consisting of only a few hundred atoms. It is distinct from CNT and DFT in its treatment of the nucleus and the surrounding media, as illustrated in **Figure 2**. Following a brief discussion of experimental methods, we devote the rest of this review to molecular simulations and leave further progress in DFT to interested readers.

EXPERIMENTAL METHODS

Homogeneous crystal nucleation occurs in the interior of a supercooled liquid, which makes it difficult for any experimental equipment to detect. Moreover, even small amounts of impurities induce heterogeneous nucleation that quickly drives the whole system to crystallize. Vonnegut (28) proposed the droplet technique to address this problem, and Turnbull (29) used it subsequently with much success. In this technique, the sample liquid is dispersed into a large number of tiny droplets, each of which is typically approximately 1 μm in diameter, that vastly exceeds the number of impurities in the liquid. A significant number of droplets are therefore impurity free and unaffected by heterogeneous nucleation of this type. These impurity-free droplets can be used to study homogeneous nucleation. The volume of each droplet is small enough, and the growth rate of the crystal nucleus fast enough, that a single nucleation event automatically precludes other nucleation events within the same droplet and leads to nearly instantaneous crystallization of the droplet. However, the droplet must not be so small that heterogeneous nucleation initiated at the surface of the droplet becomes significant. Special procedures thus must be taken to ensure that nucleation takes place within the interior of the droplet. One simple test is to check whether the nucleation rate is proportional to the volume of the droplets or to their surface area (30). The crystallization process can be monitored using X-ray scattering, dilatometry, differential scanning

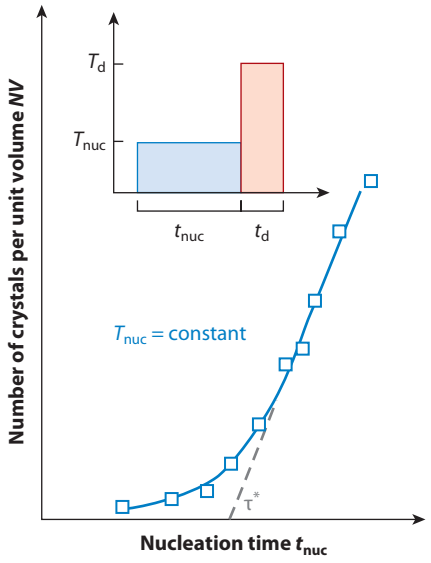

Figure 3

The number of crystals per unit volume as a function of nucleation time. The intercept of this curve on the time axis, τ^* gives the experimentally measured induction time. T_{nuc} is the nucleation temperature, and T_d is the developing temperature. Reprinted from Reference 31. Copyright © 1993, with permission from Elsevier.

calorimetry, or visual methods. By these techniques, one can measure directly the induction time for the homogeneously nucleated droplets and from this estimate determine the homogeneous nucleation rate *I*. The induction time τ^* can be estimated by extrapolating the linear portion of a plot of the measured number of crystals per unit volume versus time to the time axis, as illustrated in **Figure 3**. To calculate *I* from the induction time measurement, one must first estimate the magnitude of τ'. Skripov (2) has performed this estimation by making use of the fact that stationary nucleation is a random event process and that the distribution of waiting time to observe a nucleation event should follow an exponential distribution, as expected of a Poisson process. The Poisson process has the important property that the probability of occurrence of an event should be independent of the time origin when measurements begin. Using this, it is possible to determine the magnitude of the time lag τ', during which stationary nucleation does not hold, and thus subtract it from the experimental measurement of τ^*. Numerical methods to estimate τ^* and τ' are presented in the Simulation Methods section below.

Unlike the vapor-liquid transition, at which the interfacial free energy is equal to the interfacial tension and is relatively easy to measure, solid-liquid interfacial free energies are quite difficult to measure, especially away from coexistence. The available data are rare (32). Within the limitations of CNT, the homogeneous nucleation experiment allows one to measure a solid-liquid interfacial free energy. Several different methods can be used depending on whether the nucleation occurs isothermally or with a finite cooling rate.

For isothermal nucleation experiments, combining Equations 2, 5, and 9, one obtains

$$\ln I = \ln I_0 - \frac{16\pi}{3k_B}\frac{T_m^2\sigma^3}{\rho_n^2\Delta H_f^2}\frac{1}{\Delta T^2 T}. \qquad 18.$$

Therefore, if the nucleation rate I is measured as a function of temperature, the interfacial free energy σ can be obtained from the slope of a plot of ln I against $1/\Delta T^2 T$, and the kinetic prefactor I_0 is obtained from the intercept. Turnbull and coworkers (33) adopted this method to measure the interfacial free energy σ for various organic and inorganic materials. For nucleation experiments with a finite cooling rate, an alternative approach has been proposed (33). A supercooling experiment is performed with cooling rate r_1, and a specified fraction of droplets is solidified in the system when the temperature is lowered from T_m to T_1. Using a higher cooling rate r_2 will result in a lower temperature T_2 required instead of T_1 for the same fraction of droplets to solidify. The difference in the cooling rates and the respective supercooling are related through the critical free energy ΔG^* by

$$\ln\left(\frac{r_1}{r_2}\right) = \frac{2\Delta G^* \Delta T_d}{k_B T\, \Delta T_{av}}, \qquad 19.$$

where $T = (T_1+T_2)/2$, $\Delta T_{av} = T_m - T$, and $\Delta T_d = T_2 - T_1$. Once the critical free energy ΔG^* is obtained from Equation 19, the interfacial free energy σ can be calculated using Equations 2 and 5.

SIMULATION METHODS

With the development of computer technology and advanced algorithms, molecular simulation has become an increasingly valuable tool for the study of condensed systems, allowing scientists to study structure and dynamics with atomic-scale resolution. In order of increasing complexity, the Ising model (34), hard-sphere model (35), soft-sphere model (36), and Lennard-Jones model (37) are among the most frequently studied because of their simplicity and universality for large groups of real systems. Molecular simulation methodologies can be divided into two main classes, depending on whether they target primarily the thermodynamics or the kinetics of the nucleation phenomena, respectively.

Order Parameters and Reaction Coordinate

Order parameters are used to distinguish one phase from another. For the liquid-vapor transition, it suffices to consider the fluid density as the order parameter. For the liquid-solid transition, symmetry changes as well as density, and more sophisticated order parameters are needed. Ramakrishnan & Yussouff (38, 39) proposed the Fourier components of density, ρQ's, as order parameters in solid-liquid phase transitions. These order parameters were used by Alexander & McTague (40) to construct a Landau free energy functional for the purpose of determining the relative stability between bcc and fcc crystal structures. These ρQ's are not associated with a particular position or particle; they are properties of the bulk phase and serve as coarse-graining variables in Landau's theory.

Mandell et al. (41) used a local structure factor, $S(k, r, R)$, to define a crystal region, but the resolution is generally not good enough for use in particle-based simulations, and furthermore its value is sensitive to the orientation of the crystal nuclei. Voronoi polyhedra can be used to associate a volume of space with each particle and have been used to distinguish solid-like particles from liquid-like particles (36, 42–46). The drawback of the Voronoi analysis is that it is time-consuming. More significantly, the Voronoi signature of each crystal structure often is a histogram of polyhedra. These histograms can change significantly owing to small thermal vibrations of the lattice, which makes the Voronoi method less robust for analyzing small crystal objects. For example, the rhombic dodecahedron that is a signature of the fcc lattice is rapidly lost under tiny thermal vibrations.

Taking advantage of the observation by Haymet (47) that the Lennard-Jones solid contains many nearly collinear triplets of neighboring particles (e.g., 12 nearest neighbors, or 6 collinear triplets, in the perfect fcc or hcp lattice), Honeycutt & Andersen (48) defined a solid-like particle as one with at least five such triplets whose angles are within a cutoff angle near 180°. However, the nucleus size thus defined is quite sensitive to the cutoff angle. Also taking advantage of the correlation between the neighboring bonds, Steinhardt et al. (49) designed a set of bond orientational order parameters $q_l(i)$ using the spherical harmonics $Y_{lm}(\theta, \phi)$ of each bond that joins particle i and one of its nearest neighbors. The bond orientational order parameters allow the assignment of single particles to one phase or another. These order parameters are invariant under rotation of the crystal nuclei. Furthermore, they are large for all crystal structures and vanish for disordered phases. In particular, q_6 is unusual in that its value is almost the same for the most common fcc, hcp and bcc structures, and thus serves well to distinguish crystals from melt without regard to a specific crystal structure. The particle averages of local order parameters $q_l(i)$ are the global order parameters, Q_6, Q_4, etc., that are used to measure the overall degree of crystallization of the system. The Steinhardt bond orientational order parameters have seen widespread use in nucleation studies of various systems, including soft spheres (36, 50), Lennard-Jones particles (46, 51, 52), hard spheres (35), molecular nitrogen (53, 54), the Yukawa system (55), CO_2-water mixtures (56), sulfur hexafluoride (57), sodium chloride (58), and diamond (59). Nosé & Yonezawa (51) compared Voronoi parameters with bond orientational order parameters and found that the latter are more sensitive to the phase transition.

Other order parameters have been proposed for studies of crystal nucleation. A tetrahedral order parameter for water-like molecules (60) was used by Radakrishnan & Trout (56) in the study of ice nucleation in CO_2-water mixtures. A nematic order parameter (61) was used in studying the solid-liquid phase transition in anisotropic molecular systems, e.g., hard rods (62) and *n*-alkanes (63, 64). Beckham et al. (65) used the local aspect ratio of the unit cell to identify different solid phases of terephthalic acid. Santiso & Trout (66) developed a general set of structural order parameters for organic molecular crystals and applied them in the study of homogeneous crystal nucleation of benzene from the melt (67).

Once the phase of each particle is defined, neighboring groups of similar particles can be associated into a nucleus using conventional clustering algorithms. In this way, not only the crystallinity of the system but also the sizes of crystal domains, or nuclei, are determined. In some cases, identification of neighboring crystal sites is part of the process of defining whether a site is crystalline or not (63). More generally, however, a cutoff distance based on crystal lattice packing or molecular size is used to identify nearby sites for potential aggregation into a single cluster or nucleus. Invariably, some arbitrariness occurs in choosing these cutoffs, which can be mitigated by the use of other physical quantities to calibrate the cluster definition. For example, the percolation temperature has been used to validate the cluster definition in the Ising model (68), and the nucleation rate has been used with the Ising model (69, 70) and the Lennard-Jones model (71, 72) to define cluster size on the basis of the nucleation theorem (Equation 17).

It is useful to distinguish the concept of a "reaction coordinate" from the foregoing discussion of order parameters. The reaction coordinate, as defined in TST, refers to the actual path (or set of paths) through phase space along which a system moves from its initial state, the reactant, to its final state, the product. Generally speaking, phase space is $6N$-dimensional, where N is the number of particles. In some particularly straightforward cases, the full $6N$-dimensional space can be projected down into a lower-dimensional space defined by a small number of collective variables. Often, these collective variables are the order parameters themselves, and the reaction coordinate is assumed to be a linear combination of the collective variables (73, 74). In the study of phase transitions, it is certainly to be expected that the order parameters will vary in some

fashion as the system traverses the reaction coordinate. However, the order parameters are really just a means for distinguishing one phase from another, and there is no guarantee that they vary monotonically along the reaction coordinate. More importantly, such parameters may not capture the local nature of fluctuations that give rise to cluster formation and nucleation. For reasons such as this, it is natural to define a reaction coordinate for nucleation in terms of a local metric, such as the size of the largest nucleus in the system, n_{max}. A thermodynamic justification of this choice is presented in the Nucleation Free Energy section below. In addition, n_{max} has been used to signal the onset of nucleation in a variety of systems, e.g., Ising (75), Lennard-Jones (45), *n*-alkanes (63), and water (76).

Nucleation Free Energy

Thermodynamic approaches to nucleation rely on sampling of the free energy surface. In this way, not only can one determine the relative stability of different states, but also the transition states can be identified as first-order saddle points on the free energy surface. The minimum energy path (MEP) from a metastable state to a more stable one via one or more transition states defines the reaction coordinate. In practice, the free energy is sampled as a function of a few well-chosen collective variables by which the reaction coordinate is well defined.

The Monte Carlo method is suitable for free energy sampling. Biasing techniques are frequently employed to improve the sampling efficiency because nucleation is a rare event that often requires the crossing of a high free energy barrier. Among them, the most well known is the umbrella sampling method (77, 78), which imposes an artificial biasing potential on the system so that the phase space in the vicinity of the transition state, where the Boltzmann factor is small, is statistically well sampled. The biasing potential is a function of one or more biasing parameters. A good biasing parameter closely approximates the reaction coordinate; therefore, when the system is driven using the biasing parameter, one is actually sampling phase space along the reaction coordinate, which is also most relevant to the actual transition process.

The umbrella sampling method has been used successfully in many nucleation studies. Early studies of crystal nucleation used global order parameters such as Q_6 as the biasing parameter, e.g., in soft-sphere (36) and Lennard-Jones systems (46, 52). Because Q_6 does not distinguish between several common crystal structures, it permits the development of polymorphism as part of the nucleation process. However, two problems have been identified with using a global order parameter such as Q_6 as the biasing parameter. First, the value of Q_6 at the transition state, and the corresponding critical free energy, is a function of system size (53), which makes it an extensive property that varies from system to system. Second, there arises the possibility of a phenomenon called entropic breakdown (79), in which a system with a given Q_6 prefers to organize as a collection of numerous small nuclei rather than a single large nucleus. These two problems occur because Q_6 is not a good approximation of the reaction coordinate. Nucleation is intrinsically a local event, the presence of which is not uniquely or sensitively identified by a global order parameter unless the system itself is tiny. For these reasons, despite efforts to improve upon global order parameters (54, 80), it has become increasingly common practice to employ the locally defined quantity n_{max} as the reaction coordinate, thereby also defining the biasing parameter (35). Using n_{max} as the biasing parameter in umbrella sampling Monte Carlo simulation, Auer & Frenkel (35) sampled the free energy of nucleation, as shown in **Figure 4**. It has the shape predicted by CNT.[1]

[1]The *n* employed in **Figure 4** and References 79 and 102 refers to the largest cluster in the system, which we call n_{max} here. As explained in the text, the distinction is important.

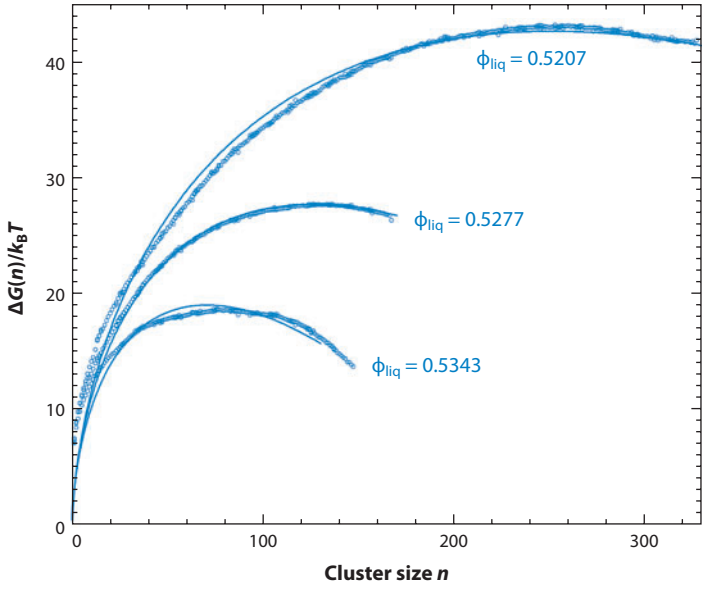

Figure 4

The calculated free energy barrier for homogeneous crystal nucleation of hard-sphere colloids. Results are shown for three values of the volume fraction of the colloids in the liquid phase; $\phi_{liq} = 0.5207$, 0.5277 and 0.5343. The barrier was computed using Equation 6. According to the original work, n here is used synonymously with n_{max}. Reprinted by permission from Macmillan Publishers Ltd from Reference 35; copyright © 2001.

More recently, a method called metadynamics (MTD) (81) has been employed to study nucleation. It also introduces biasing potentials to improve the sampling efficiency, in the form of superposed Gaussian functions centered at previously sampled state points. As a result, the biasing potential is history dependent. To be effective, MTD relies on coarse-graining parameters, which must be chosen with care, to define the biasing potentials. Such biasing schemes have been implemented in publicly available molecular dynamics (MD) software such as LAMMPS (82) and GROMACS (83). The coarse-grained biasing parameter must be an explicit function of particle coordinates to facilitate the calculation of the biasing force as a function of the spatial gradients of the biasing parameters. For example, Trudu et al. (80) used MTD to sample the free energy in a Lennard-Jones system. They chose the potential energy and a local Q_6 as biasing parameters. The local Q_6 was introduced to approximate n_{max} to avoid the aforementioned problems of global order parameters.

The difference between n, the size of any nucleus in the system, and n_{max}, the size of the largest nucleus in the system, is subtle but important. The free energy $\Delta G(n)$ introduced in CNT is defined as the system free energy change owing to the change in the size of the single nucleus in the system, as illustrated in **Figure 5*a***, for which n and n_{max} are equivalent. Naturally, $\Delta G(n) = 0$ when $n = 0$, and the critical free energy defined in CNT is $\Delta G^*(n) \equiv \Delta G(n^*)$, as in Equation 2. However, when a real system is supercooled and nuclei are identified as described in the Order Parameters and Reaction Coordinate section above, there is always a distribution of nuclei of finite size in the metastable state, as shown in **Figure 5*b***, and one is forced to select some characteristic of the several nuclei, such as n_{max}, as the reaction coordinate; in this case, n and n_{max} are not equivalent. In this case, $\Delta G(n_{max})$ is defined as the system free energy change owing to the change in the size of the largest nucleus in the system. The reference state for $\Delta G(n_{max})$ is chosen to

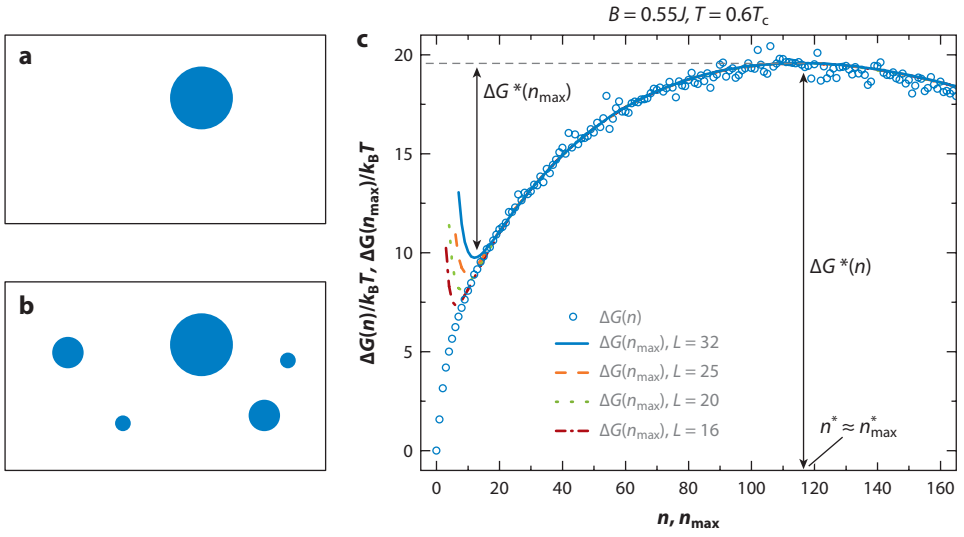

Figure 5

The free energy of a system according to classical nucleation theory. (*a*) A system containing only one nucleus. (*b*) A system containing multiple nuclei, the largest of which has size $n_{\max}$. (*c*) $\Delta G(n)$ and $\Delta G(n_{\max})$ as a function of n and $n_{\max}$, respectively. For purposes of comparison, the $\Delta G(n_{\max})$ curves have been shifted vertically to match the $\Delta G(n)$ curve near $n = n^*$.

be the metastable equilibrium state, where $n_{\max}^{\mathrm{mp}}$ is the most probable value of $n_{\max}$ and corresponds to the minimum of $\Delta G(n_{\max})$ for $n_{\max} < n_{\max}^*$. Under most circumstances, $n_{\max}^{\mathrm{mp}}$ is not zero. When the largest nucleus is much larger than the rest of the nuclei, the $\Delta G(n_{\max})$ curve is expected to approximate the $\Delta G(n)$ curve closely, i.e., the free energy change of the system is dominated by the largest nucleus, and the other nuclei serve only as part of the background medium. If we define n' as an effective upper limit on nucleus size observed in the system in its metastable equilibrium state, then when $n_{\max} \gg n'$, $\Delta G(n_{\max})$ is indeed well approximated by $\Delta G(n)$; however, if $n_{\max} \leq n'$, then the metastable equilibrium distribution of nuclei affects the estimation of $\Delta G(n_{\max})$ so that the latter deviates from $\Delta G(n)$. We illustrate the difference between $\Delta G(n)$ and $\Delta G(n_{\max})$ using the 3D Ising model in the example that follows.

The Ising model is one of the most commonly used lattice models. The discrete positions of spins and the simple form of interaction make computation much less costly compared with off-lattice models, and analytical results are often available. Binder and coworkers (34, 84) have carried out extensive theoretical and simulation studies on nucleation using the Ising model. It still serves as a good model for testing nucleation methods (68–70, 85–88).

A cubic lattice with side length L, such that the whole system contains $L \times L \times L$ spins, was used. Periodic boundary conditions were applied to all three dimensions. The Hamiltonian of the system is expressed by

$$\frac{H}{k_{\mathrm{B}}T} = -\frac{J}{k_{\mathrm{B}}T}\sum_{<i,j>} s_i s_j - \frac{B}{k_{\mathrm{B}}T}\sum_i s_i, \qquad 20.$$

where the first sum runs over all nearest-neighbor pairs and the second sum runs over all sites. J is the interaction coefficient, and B is the magnetic field. The critical temperature for the 3D Ising model is $k_{\mathrm{B}}T_{\mathrm{c}} \approx 4.51J$. The system was initially configured with all down spins and $T = 0.6T_{\mathrm{c}}$ so

that the initial configuration was stable. Then, the system was rendered metastable with respect to its counterpart having all up spins by applying a magnetic field B. A nucleus then consists of a cluster of up spins connected through nearest-neighbor interactions. The Metropolis algorithm was used to sample configuration space, flipping one spin at a time. One observes, as is typical of nucleation, that the system remains in the metastable state for many Monte Carlo steps before a critical nucleus of up spins drives the spin system to a complete reversal.

Using umbrella sampling Monte Carlo with $n_{\max}$ as the biasing parameter, we sampled the free energy of the system, $\Delta G(n_{\max})$, as a function of $n_{\max}$. $\Delta G(n_{\max})$ was calculated from the probability, $P(n_{\max})$, of observing a system with a given value $n_{\max}$, after bias correction,

$$\Delta G(n_{\max})/k_{\mathrm{B}}T = -\ln[P(n_{\max})/P(n_{\max}^{\mathrm{mp}})]. \quad 21.$$

Because the system always contains multiple nuclei of various sizes, $\Delta G(n)$ can also be interpreted as the relative free energy between nuclei of different sizes and calculated using the ensemble-averaged probability $P(n)$ of observing nuclei of size n in the system, according to Equation 22 (46, 88):

$$\Delta G(n)/k_{\mathrm{B}}T = -\ln[\langle P(n)\rangle/\langle P(0)\rangle], \quad 22.$$

where $\langle P(n=0)\rangle$ can be estimated by extrapolation. According to this interpretation, it is reasonable to call $\Delta G(n_{\max})$ the system free energy and $\Delta G(n)$ the nucleus free energy, for distinction. The free energies $\Delta G(n_{\max})$ and $\Delta G(n)$ obtained in these simulations are shown in **Figure 5*c***. $\Delta G(n)$ has the shape predicted by CNT. However, $\Delta G(n_{\max})$ has a local minimum at a small but finite $n_{\max}^{\mathrm{mp}}$, owing to the entropic contribution from multiple nuclei. Nevertheless, the free energy curves for $\Delta G(n_{\max})$ and $\Delta G(n)$ overlap in the vicinity of the critical nucleus, i.e., $n_{\max}^{*} \approx n^{*}$. This serves to confirm that the mechanism is mononuclear and that n^{*} is well approximated by $n_{\max}^{*}$ in this case.

Figure 5*c* also demonstrates that $\Delta G(n_{\max})$ is system-size dependent, mainly owing to the system-size dependence of $n_{\max}^{\mathrm{mp}}$, whereas $\Delta G(n)$ is not. When the system size is large compared with the crystal nuclei, the system free energy barrier $\Delta G^{*}(n_{\max}) \equiv \Delta G(n_{\max}^{*})$, illustrated in **Figure 5*c***, could be small. These Ising model simulations confirm the following relationship:

$$\Delta G^{*}(n_{\max}) = \Delta G^{*}(n) - k_{\mathrm{B}}T\ln V, \quad 23.$$

where $V = L^3$ is the volume of the system. The result of a small $\Delta G^{*}(n_{\max})$ is a very fast phase transition because the chance of finding a critical nucleus increases with increasing system size. The observation of faster phase transitions in larger systems has on occasion been mistakenly interpreted as spinodal decomposition. Trudu et al. (80) used MTD to sample the free energy as a function of local Q_6 and the potential energy and found that the free energy barrier vanished at $T/T_{\mathrm{m}} = 0.64$. However, Bartell & Wu (89) and Peng et al. (90) showed that the phase transition was still nucleation mediated. **Figure 5*c*** illustrates that with increasing system size, $\Delta G^{*}(n_{\max})$ can become vanishingly small, even though $\Delta G^{*}(n) > k_{\mathrm{B}}T$ is still satisfied and the classical nucleation mechanism prevails.

As a final note, Equation 23 provides a means for recovering Equation 9 of CNT from simulations using $n_{\max}$ as the reaction coordinate. If we assume that the true nucleation rate is that obtained by simulation normalized simply by volume, then

$$I = \frac{I_0}{V}\mathrm{e}^{-\Delta G^{*}(n_{\max})/k_{\mathrm{B}}T} = I_0\mathrm{e}^{-\Delta G^{*}(n)/k_{\mathrm{B}}T} = I_0\mathrm{e}^{-\Delta G^{*}/k_{\mathrm{B}}T}, \quad 24.$$

and Equation 9 is recovered. Equation 24 serves as a justification for using $n_{\max}$ as the reaction coordinate in nucleation studies. The difference between $\Delta G(n_{\max})$ and $\Delta G(n)$ has also been discussed elsewhere (91–93).

Simulations that sample the free energy surface allow one to evaluate the entire free energy curve, $\Delta G(n)$ versus n. By contrast, experiments permit the measurement of only a single value, ΔG^* or $\Delta G\,(n^*)$. The latter can be used to calculate the interfacial free energy σ if one assumes that the critical nucleus is spherical (35, 94). However, for many real systems, a spherical nucleus seems overly simplified. More complex and interesting models such as the cylindrical nucleus can be tested using simulation results, by fitting to the entire free energy curve. Using a cylindrical model, the end surface and side surface can be distinguished, and the respective free energy values σ_e and σ_s can be calculated, e.g., for a system of anisotropic molecules (64, 95).

Crystal polymorphism and Ostwald's rule. Polymorphism among molecular crystals is an interesting phenomenon (96) and is of great interest in many disciplines, including crystal chemistry, materials science (97), and pharmaceutical science (98). An important development in polymorphism came with the famous rule of stages proposed by Ostwald (99), which states that the transformation of an unstable (or metastable) system into a stable one need not proceed directly to the most stable configuration, but rather may proceed by one or more intermediate configurations that are also metastable but have free energies closer to the preceding, or initial, state. Several attempts have been made to provide thermodynamic explanations for Ostwald's rule by calculating relative stabilities between polymorphs on the basis of Landau's theory (40, 100). However, molecular simulations provide a means for studying the structure of critical nuclei and the dynamics of the formation (using MD) of polymorphs in even more detail, and polymorphism has been found to be quite common. In simulations of the Lennard-Jones system, a metastable bcc phase is nucleated, which is then transformed into a more stable fcc phase. Furthermore, ten Wolde et al. (46, 52) found that the transformation from bcc to fcc takes place before the critical nucleus is reached. As the nucleus grows up to and beyond the critical size, the core of the nucleus exhibits an fcc-like structure, whereas the diffuse interface of the nucleus exhibits a bcc-like structure (46, 52). Auer & Frenkel (35) also found that the hard-sphere fluid nucleates into the metastable random hexagonal close-packed (rhcp) structure. Only later does this metastable structure transform into the stable fcc structure. Leyssale et al. (53) reported similar observations in their simulation of molecular nitrogen, in which the analysis of the critical nucleus showed that nucleation occurred through the metastable fcc-like α phase rather than the stable hcp-like β phase. In subsequent studies (54, 101), however, they found that the metastable structure formed during the nucleation did not transform into the stable structure. Rather, the fcc-like α phase and hcp-like β phase coexist and both grow; the metastable α phase grows at a slower rate.

Moroni et al. (102) used the transition path sampling and umbrella sampling methods to study the same Lennard-Jones system as ten Wolde et al. (52), and found many different transition pathways with critical nuclei that varied from small, compact, fcc clusters to large, less well-ordered, more bcc-like structures. Desgranges & Delhommelle (55, 103) changed the relative stability between fcc and bcc structures in charge-stabilized colloid suspensions by modifying the value of the screening parameter λ in the Yukawa potential; their simulations showed that, regardless of the relative stability of the bcc and fcc phases, nucleation proceeds first into the bcc phase, and that only during the growth stage does the crystal transform into the more stable phase. This reaffirms that kinetics and the relative free energy of the critical nuclei give rise to Ostwald's rule of stages.

Metastable polymorphs can serve as intermediate states during crystallization in more complicated molecular systems as well. For example, a less stable rotator phase can facilitate crystal nucleation in *n*-alkane melts (104), and a structure with hexagonal packing precedes the formation of the final stable orthorhombic structure in polyethylene crystallization at high pressure (105). On a much larger length scale, long *n*-alkanes crystallize into lamellae with an integer

number of polymer crystal stems per chain, which are also believed to be metastable with respect to the fully extended chain crystallite. Such lamellae are normally long lived, but in some long *n*-alkanes, transformations from twice-folded to once-folded, or once-folded to fully extended, crystallites have been observed (106). More recently, it has been argued that such less-than-fully extended crystalline lamellae are actually the thermodynamically most stable state (107). The role of these polymorphs, or metastable states, in polymer crystallization is an active research topic (108).

Other free energy sampling methods. Other free energy sampling methods include parallel tempering, also known as replica exchange (109), and the blue-moon ensemble (110). Recently a method using Jarzynski's equality has been developed that allows the calculation of equilibrium free energy from nonequilibrium work. It is similar to thermodynamic integration methods, but it does not require equilibration at each point on the path. This method was used to study DNA folding (111) and to calculate the planar interfacial solid-liquid free energy in a Lennard-Jones system (112).

Nucleation Kinetics

As suggested by Ostwald's rule, the kinetics of nucleation ultimately determines the sequence of events that leads to phase change. On the one hand, characterization of the free energy surface is informative, but it requires invocation of a theory such as TST to construct a rate equation. MD, on the other hand, provides the opportunity to sample transitions without bias. Under favorable circumstances, a collection of such transition paths can be obtained for the study of the transition mechanism. By its nature, MD samples most accurately in the microcanonical ensemble. However, simulations in which the system density and energy are held constant are generally suspect because these constraints may hinder or suppress altogether the formation of a stable nucleus of a denser, lower energy phase. For this reason, simulations at constant pressure and, usually, constant temperature are preferred.

Mandell et al. reported the first MD study of crystal nucleation using a Lennard-Jones system (37). They used a small system of 108 particles with periodic boundary conditions. The small size of the system used raised questions of finite size effects in nucleation. The finite size effect was examined by Honeycutt & Andersen (48), and Swope & Andersen (45) reported further simulations using 15,000 and then 10^6 Lennard-Jones particles. They measured the steady-state nucleus size distribution $P_{st}(n)$. They then fitted $P_{st}(n)$ to a polynomial and, by finding the maximum of $P_{st}(n)$, they estimated the critical nucleus size n^*. However, $P_{st}(n)$ should decrease monotonically, as shown in **Figure 6**. The critical nucleus size n^* can be found by locating the minimum of $P_{eq}(n)$, which is related to $P_{st}(n)$ by (see equation 13.2 in Reference 5)

$$P_{st}(n) = P_{eq}(n)\frac{\{1 - \mathrm{erf}[Z\sqrt{\pi}(n - n^*)]\}}{\{1 - \mathrm{erf}[Z\sqrt{\pi}(1 - n^*)]\}}. \qquad 25.$$

The difference between $P_{st}(n)$ and $P_{eq}(n)$ is shown in **Figure 6**. To calculate $P_{st}(n)$, and thus $\Delta G(n)$, from $P_{eq}(n)$, or vice versa, prior knowledge of n^* is needed.

An alternative method to determine the critical nucleus size n^* takes advantage of the equal probability of a critical nucleus to either grow or decay. This principle was applied to determine the critical nucleus size n^* for the Ising model (70) and the Lennard-Jones system (72, 94). This method has the advantage that one need not run a long simulation to determine whether a nucleus is critical or not. However, the method does not resolve the problem of generating appropriate nuclei in the first place. Bai & Li (94) prepared systems containing a nucleus embedded into a

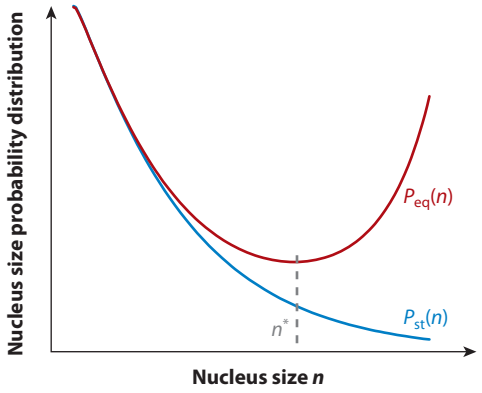

Figure 6

Equilibrium nucleus size probability distribution $P_{eq}(n)$ and steady-state nucleus size probability distribution $P_{st}(n)$.

liquid, but it is difficult to know whether the nuclei thus formed have the same shape, structure, and surface as those that grow naturally in the supercooled liquid. In all likelihood, the critical nucleus does not have a unique shape and structure, but rather the critical state comprises an ensemble of such nuclei.

The induction time τ^* is a signature of a nucleation event, and of rare events in general, and is readily evaluated in an MD simulation. During the induction period, not just some, but all system variables should fluctuate around averages that are characteristic of the metastable equilibrium state. Lack of a clear induction period may be a sign of preexisting supercritical nuclei (owing to system size, for example) or that the spinodal has been crossed. For the MD simulations in which nucleation can be observed, a nucleation rate can be calculated from the induction time using Equation 13. The nucleation rate then can be used to determine a parameter-free nucleus size by using the nucleation theorem. This approach has been applied to the Ising model (69, 70) and the Lennard-Jones model (71, 72). A more systematic procedure to identify the critical nucleus size through MD simulation is that based on mean first-passage time (MFPT) analysis (113–116).

Mean first-passage-time analysis. The MFPT method was proposed to determine the induction time and to extract other useful thermodynamic information directly from MD simulations of nucleation (113–116). This class of methods has been independently developed and presented in various forms by several groups, but they are essentially correlated (117). Here we discuss the approach reported by Wedekind et al. (116), which is based on a calculation by Hänggi et al. (113) and makes particularly clear the link between the classical theoretical treatment and the quantities available from MD simulation. Hänggi et al. (113) defined the MFPT $\tau(x)$ as the average time elapsed until the process starting at state point x leaves a prescribed domain for the first time. For studies of nucleation, x can be equated with the reaction coordinate, n_{max}. Practically speaking, in one MD trajectory, any $n_{max} < n^*_{max}$ belongs to the phase space of the metastable equilibrium state and may be visited multiple times before a critical nucleation event occurs. Therefore, the mean refers to the average of different states that have the same n_{max}. Wedekind et al. (116) reinterpreted the MFPT $\tau(x)$ to be the time before x is visited for the first time. For one MD trajectory, there is only one measurement of $\tau(x)$ for each x, and the mean is the average over multiple MD trajectories.

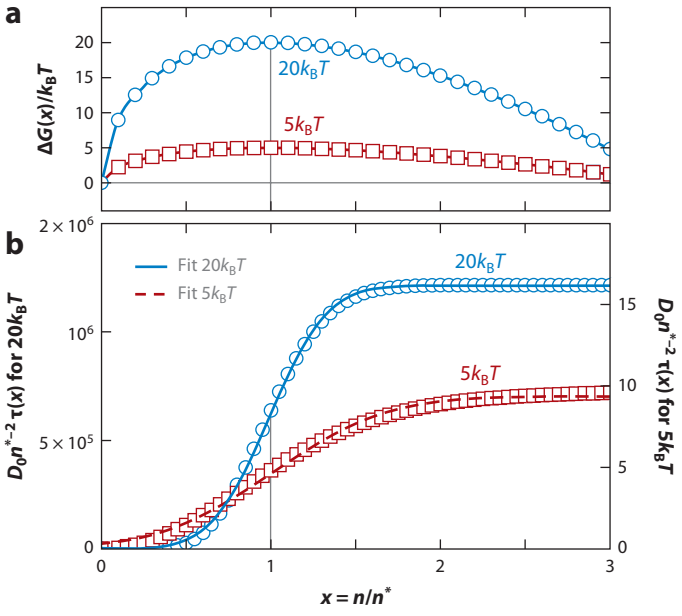

Figure 7

(*a*) Two free energy barriers of $5k_BT$ and $20k_BT$; (*b*) corresponding mean first-passage times (symbols) and their fit to Equation 26. D_0 is the constant diffusion coefficient. Reprinted with permission from Reference 116. Copyright © 2007, American Institute of Physics.

For processes with sufficiently high barrier energies (relative to k_BT), the MFPT of n_{max} takes the approximate form

$$\tau(n_{max}) = 0.5\tau^*\{1 + \mathrm{erf}[Z\sqrt{\pi}(n_{max} - n^*_{max})]\}, \quad 26.$$

where τ^* is the induction time and Z is the Zeldovich factor,

$$Z = \sqrt{\frac{1}{2\pi k_BT}\left|\frac{d^2\Delta G(n_{max})}{dn^2_{max}}\right|}. \quad 27.$$

The critical value n^*_{max} corresponds to the transition state. Therefore, MFPT analysis allows us to estimate n^*_{max}, Z, and τ^* from MD simulations. This method is illustrated in **Figure 7**. Because the simulation box is usually quite small, the simulated nucleation process occurs predominantly by the mononuclear mechanism. One can take advantage of this to calculate the nucleation rate I using Equation 13 and then use its value to predict τ^* in a much larger system on the basis of Equation 15.

In practice, even an instantaneous quench to a supercooled state in an MD simulation gives rise to a period in which nonstationary nucleation can occur. The measured induction time should then be corrected for the time lag τ' associated with this period. Basically, τ' is the time required for the system to reach the stationary nucleation condition. In the melt, τ' is proportional to the viscosity η of the melt and can be substantial. We have analyzed the induction time in *n*-alkanes and found a significant time lag for *n*-alkanes as short as *n*-eicosane (C20). Using the method proposed by Skripov (2), we have estimated the magnitude of τ'. As shown in **Figure 8**, for an *n*-eicosane melt, τ' is approximately 10 ns (95), whereas in a melt of a longer *n*-alkane with 150 carbons on each

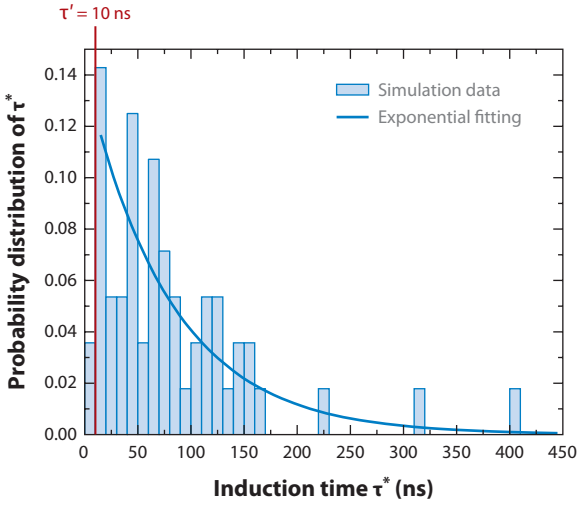

Figure 8

The probability distribution of the induction time in an *n*-eicosane melt at approximately 20% supercooling; $\tau' = 10$ ns is the minimum time lag such that the probability distribution of $(\tau^* - \tau')$ follows the Poisson distribution. Reprinted with permission from Reference 95. Copyright © 2011, American Institute of Physics.

chain (C150), τ' may be as large as 200 ns (P. Yi & G.C. Rutledge, unpublished results). As is evident from the C150 example, the time lag τ' may dominate experimental measurement of the induction time; thus, the nucleation rate calculated by Equation 13 is also affected by τ'.

We have used the MFPT method and the free energy sampling method to estimate the critical nucleus size n^* for several *n*-alkane systems, and the results are consistent (64, 95). The MFPT method was furthermore extended by Wedekind and colleagues (93, 118) to reconstruct the free energy curve of the system $\Delta G(n_{max})$ using the steady-state probability distribution of n_{max}, $P_{st}(n_{max})$, and the MFPT of n_{max}, assuming steady-state nucleation.[2]

The MFPT method is not limited to nucleation but rather is generally applicable to rare event processes for which a suitable reaction coordinate is identified. It has the advantage that it may be applied in general to any unbiased MD simulation trajectory once the reaction coordinate is chosen. Practically speaking, however, unbiased MD simulations require exceedingly long times to sample truly rare events accurately. Furthermore, given the exponential nature of the induction time distribution, the induction time must be averaged over a large number of independent trajectories to have any statistical significance. For these reasons, its applicability to systems close to coexistence, i.e., with very high nucleation free energy barriers, is limited. Below we discuss some other methods to calculate the nucleation rate with high nucleation free energy.

Advanced methods to calculate nucleation rate. With currently available technology, the timescale accessible to molecular simulations is normally on the order of picoseconds to nanoseconds, far shorter than the induction time in real experiments. Furthermore, the induction time is inversely proportional to the system volume (Equation 13), which makes the direct observation of

[2]Although the authors initially (116) used nucleus size *n* rather than n_{max} as the reaction coordinate, it was corrected later (93).

nucleation in MD simulation very difficult. To simulate homogeneous nucleation, the supercooling usually must be quite large. For example, Swope & Andersen (45) studied the Lennard-Jones system at 50% supercooling. More recently, homogeneous crystal nucleation has been observed in water at approximately 15% supercooling (76) and in *n*-alkanes at approximately 20% supercooling (64, 95). The same difficulty is also encountered in the study of protein folding (119). For complex molecules such as *n*-alkanes and proteins, quite often a coarse-grained force field is used to speed up the computation.

When brute force MD simulation is impractical, biasing methods such as umbrella sampling and metadynamics can accelerate the occurrence of rare events by changing the free energy barrier, but then the transition rate will not be as accurate. An alternative approach is the linear response method of Bennett (120) and Chandler (121). Assuming that the actual transition time is much faster than the induction time, this method decomposes the nucleation rate into the product of the exponential of the critical free energy and the kinetic prefactor. The critical free energy can be obtained from free energy sampling as discussed in the Nucleation Free Energy section above, whereas the kinetic prefactor can be calculated from MD simulations in which the system is prepared initially at the top of the free energy barrier (46). The kinetic prefactor can also be evaluated using the Monte Carlo method (35) if the Monte Carlo moves are chosen such that all moves represent approximately equal periods of elapsed time. The Monte Carlo step can then be mapped to real time by matching, e.g., the mean square displacement (122). The robustness of this method lies in the fact that the estimated value of the reaction rate does not rely on the precise determination of the location of the transition state. Therefore, the Bennett-Chandler method remains among the most generally useful methods for calculating the transition rate constant.

When the free energy barrier is broad and shallow, or diffuse, the reaction coordinate can be hard to identify; in particular, a single reaction coordinate no longer dominates the nucleation mechanism, but rather many viable transition paths as well as numerous saddle points may exist. For cases such as this, the transition path sampling (TPS) method developed by Chandler and coworkers (123) is appropriate. To start the simulation, an initial trajectory connecting the initial and the final states is needed. Using a Monte Carlo shooting scheme, one point on the initial trajectory is displaced; then, from the new point, two simulations are started, one toward each of the initial and final states. The new trajectory is collected into the transition path ensemble if it also connects the initial and the final states. TPS does not need an explicit reaction coordinate and circumvents the need to evaluate a representative free energy barrier. The reaction coordinate represents all of the probable transition paths that connect the same reactant and product. Because transition paths are observables in experiments and simulations, harvesting an ensemble of transition paths provides some insight into the reaction coordinate. This idea underlies methods to identify a reaction coordinate using TPS (74, 124).

The main disadvantage of TPS is that it is computationally expensive. Transition interface sampling (TIS) (125) and partial path TIS (PPTIS) (126) have been proposed to remedy this problem. In these methods, a series of nonintersecting interfaces are inserted between the initial and the final states. These interfaces are chosen in accordance with selected order parameters that distinguish the initial and the final states. By so doing, sampling is carried out in multiple small steps between neighboring interfaces rather than by requiring a system to relax all the way to the initial and final states. The success of these methods hinges, of course, on the selection of order parameters that well approximate the reaction coordinate. Other than measuring the transition rate, PPTIS also assumes the loss of time correlations in the transition paths; therefore, with the help of interfaces to measure the progress of nucleation, PPTIS was used to sample the free energy of nucleation (102, 127). For the Ising model, TPS was also used to sample the free energy landscape of nucleation (88).

TPS, TIS, and PPTIS all assume detailed balance and microscopic reversibility to arrive at an ensemble of transition paths. Thus, they are limited to systems characterized by an equilibrium distribution of transition paths. Recently, a new path sampling method called forward flux sampling (FFS) (128) has been proposed to study both equilibrium and nonequilibrium transition processes. Using FFS, Sanz et al. (129) found that the nucleation does not always follow the MEP in the liquid-solid transition of colloidal suspensions of oppositely charged particles. The nucleation rate calculated by FFS was found to be different by three orders of magnitude from that determined using the Bennett-Chandler method for diamond (59), but within one order of magnitude of the TIS result for NaCl (58).

The power of TPS-type methods lies mostly in their ability to explore a reaction coordinate with high dimensionality. Although powerful for some problems, the evidence to date suggests that the nucleation of crystals from the melt can be represented by a rather simple reaction coordinate based on nucleus size. Nevertheless, such methods may eventually prove useful in this field.

SUMMARY AND FUTURE PERSPECTIVE

CNT remains the starting point for almost any discussion of nucleation in liquid-solid transitions. Nevertheless, it is highly oversimplified in its use of the capillary approximation and assumption of a single dominant transition state. Molecular simulation methods have been developed that relax these assumptions, thereby permitting researchers to test the validity of CNT in specific instances and to develop greater insight into the nature of nucleation and of rare event processes in general. Our goal in this review has been to summarize the current state of the art in this field, with particular attention to the application of methods to the study of nucleation of a crystalline solid from the metastable liquid state. Broadly speaking, these methods tend to be one of two types: either they seek to characterize the free energy surface between the liquid and solid domains of phase space, or they attempt to capture the kinetics of transitions between these two domains. Both approaches are powerful and find synergy in composite approaches such as the Bennett-Chandler method or the TPS class of methods. Crystal nucleation is just one example of rare event processes. The concepts and methods developed for the study of crystal nucleation can be transported to other problems, such as protein folding and chemical reaction rates, and vice versa.

Looking forward, we anticipate that molecular simulation methods will play an important role in furthering our understanding of several fundamental questions that currently arise in studies of nucleation from complex liquids. The recently proposed two-step nucleation and spinodal-assisted nucleation for nucleation from solution (130), for example, suggest that the solid-liquid phase transition in a complex fluid system may be more complicated than is implied by the simple dichotomy of nucleation-and-growth or spinodal decomposition. This is a research field in which molecular simulation can make significant contributions. Furthermore, it may be evident from this review that most of the studies to date have focused on the methods and principles and used relatively simple models. An important challenge for the future is the further testing and validation of these principles and methods against real materials with complex architectures and practical applications such as high-molecular-weight polymers, pharmaceuticals, and biologics. We look forward to rapid progress in these fields through the application of molecular simulation.

DISCLOSURE STATEMENT

The authors are not aware of any affiliations, memberships, funding, or financial holdings that might be perceived as affecting the objectivity of this review.

ACKNOWLEDGMENTS

The authors are grateful to ExxonMobil Corporation for financial support during the preparation of this review.

LITERATURE CITED

1. Zettlemoyer AC, ed. 1969. *Nucleation*. New York: Dekker
2. Skripov VP. 1974. *Metastable Liquids*. Transl. R. Kondor. New York: Wiley (From Russian)
3. Oxtoby DW. 1992. Homogeneous nucleation: theory and experiment. *J. Phys. Condens. Matter* 4:7627–50
4. Debenedetti PG. 1996. *Metastable Liquids: Concepts and Principles*. Princeton, NJ: Princeton Univ. Press
5. Kashchiev D. 2000. *Nucleation: Basic Theory with Applications*. Oxford/Boston: Butterworth-Heinemann
6. Anwar J, Zahn D. 2011. Uncovering molecular processes in crystal nucleation and growth by using molecular simulation. *Angew. Chem. Int. Ed. Engl.* 50:1996–2013
7. Sear RP. 2007. Nucleation: theory and applications to protein solutions and colloidal suspensions. *J. Phys. Condens. Matter* 19:033101
8. Kelton KF. 1991. Crystal nucleation in liquids and glasses. In *Solid State Physics*, ed. H Ehrenreich, D Turnbull, pp. 75–177. New York: Academic
9. Gibbs JW. 1928. *The Collected Works of J. Willard Gibbs*. New York: Longmans-Green
10. Volmer V, Weber A. 1926. Nucleus formation in supersaturated systems. *Z. Phys. Chem.* 119:277–301
11. Becker R, Döring W. 1935. Kinetische Behandlung der Keimbildung in übersättigten Dämpfen. *Ann. Phys.* 24:719–52
12. Zeldovich JB. 1943. On the theory of new phase formation; cavitation. *Acta Physicochim. USSR* 18:1–22
13. Farkas L. 1927. Keimbildungsgeschwindigkeit in übersättigten Dämpfen. *Z. Phys. Chem.* 125:236–42
14. Uhlmann DR, Kritchevsky G, Straff R, Scherer G. 1975. Crystal nucleation in normal alkane liquids. *J. Chem. Phys.* 62:4896–903
15. Turnbull D, Fisher JC. 1949. Rate of nucleation in condensed systems. *J. Chem. Phys.* 17:71–73
16. Wölk J, Strey R. 2001. Homogeneous nucleation of H_2O and D_2O in comparison: the isotope effect. *J. Phys. Chem. B* 105:11683–701
17. Cahn JW, Hilliard JE. 1959. Free energy of a nonuniform system. III. Nucleation in a two-component incompressible fluid. *J. Chem. Phys.* 31:688–99
18. Abraham FF. 1979. On the thermodynamics, structure and phase stability of the nonuniform fluid state. *Phys. Rep.* 53:93–156
19. Oxtoby DW, Evans R. 1988. Nonclassical nucleation theory for the gas-liquid transition. *J. Chem. Phys.* 89:7521–30
20. Oxtoby DW. 1998. Nucleation of first-order phase transitions. *Acc. Chem. Res.* 31:91–97
21. Zeng XC, Oxtoby DW. 1991. Gas-liquid nucleation in Lennard-Jones fluids. *J. Chem. Phys.* 94:4472–78
22. Seok C, Oxtoby DW. 1998. Nucleation in *n*-alkanes: a density-functional approach. *J. Chem. Phys.* 109:7982–90
23. Oxtoby DW, Kashchiev D. 1994. A general relation between the nucleation work and the size of the nucleus in multicomponent nucleation. *J. Chem. Phys.* 100:7665–71
24. Kashchiev D. 1982. On the relation between nucleation work, nucleus size, and nucleation rate. *J. Chem. Phys.* 76:5098–102
25. Harrowell P, Oxtoby DW. 1984. A molecular theory of crystal nucleation from the melt. *J. Chem. Phys.* 80:1639–46
26. Shen YC, Oxtoby DW. 1996. Nucleation of Lennard-Jones fluids: a density functional approach. *J. Chem. Phys.* 105:6517–24
27. Oxtoby DW. 2003. Crystal nucleation in simple and complex fluids. *Philos. Trans. R. Soc. Lond. Ser. A* 361:419–28
28. Vonnegut B. 1948. Variation with temperature of the nucleation rate of supercooled liquid tin and water drops. *J. Colloid Sci.* 3:563–69
29. Turnbull D. 1950. Formation of crystal nuclei in liquid metals. *J. Appl. Phys.* 21:1022–28

30. Carvalho J, Dalnoki-Veress K. 2011. Surface nucleation in the crystallisation of polyethylene droplets. *Eur. Phys. J. E* 34:6
31. Deubener J, Brückner R, Sternitzke M. 1993. Induction time analysis of nucleation and crystal growth in di- and metasilicate glasses. *J. Non-Cryst. Solids* 163:1–12
32. Jones DRH. 1974. The free energies of solid-liquid interfaces. *J. Mater. Sci.* 9:1–17
33. Cormia RL, Price FP, Turnbull D. 1962. Kinetics of crystal nucleation in polyethylene. *J. Chem. Phys.* 37:1333–40
34. Binder K, Müller-Krumbhaar H. 1974. Investigation of metastable states and nucleation in the kinetic Ising model. *Phys. Rev. B* 9:2328–53
35. Auer S, Frenkel D. 2001. Prediction of absolute crystal-nucleation rate in hard-sphere colloids. *Nature* 409:1020–23
36. van Duijneveldt JS, Frenkel D. 1992. Computer simulation study of free energy barriers in crystal nucleation. *J. Chem. Phys.* 96:4655–68
37. Mandell M, McTague J, Rahman A. 1976. Crystal nucleation in a three-dimensional Lennard-Jones system: a molecular dynamics study. *J. Chem. Phys.* 64:3699–702
38. Ramakrishnan TV, Yussouff M. 1977. Theory of the liquid-solid transition. *Solid State Commun.* 21:389–92
39. Ramakrishnan TV, Yussouff M. 1979. First-principles order-parameter theory of freezing. *Phys. Rev. B* 19:2775–94
40. Alexander S, McTague J. 1978. Should all crystals be bcc? Landau theory of solidification and crystal nucleation. *Phys. Rev. Lett.* 41:702–5
41. Mandell M, McTague JP, Rahman A. 1977. Crystal nucleation in a three-dimensional Lennard-Jones system. II. Nucleation kinetics for 256 and 500 particles. *J. Chem. Phys.* 66:3070–75
42. Tanemura M, Hiwatari Y, Matsuda H, Ogawa T, Ogita N, Ueda A. 1977. Geometrical analysis of crystallization of the soft-core model. *Prog. Theor. Phys.* 58:1079–95
43. Hsu CS, Rahman A. 1979. Crystal nucleation and growth in liquid rubidium. *J. Chem. Phys.* 70:5234–40
44. Cape JN, Finney JL, Woodcock LV. 1981. An analysis of crystallization by homogeneous nucleation in a 4000-atom soft-sphere model. *J. Chem. Phys.* 75:2366–73
45. Swope WC, Andersen HC. 1990. 10^6-particle molecular-dynamics study of homogeneous nucleation of crystals in a supercooled atomic liquid. *Phys. Rev. B* 41:7042–54
46. ten Wolde PR, Ruiz-Montero MJ, Frenkel D. 1996. Numerical calculation of the rate of crystal nucleation in a Lennard-Jones system at moderate undercooling. *J. Chem. Phys.* 104:9932–47
47. Haymet ADJ. 1984. Orientational environments in liquids and solids. *Chem. Phys. Lett.* 107:77–82
48. Honeycutt JD, Andersen HC. 1986. Small system size artifacts in the molecular dynamics simulation of homogeneous crystal nucleation in supercooled atomic liquids. *J. Phys. Chem.* 90:1585–89
49. Steinhardt PJ, Nelson DR, Ronchetti M. 1983. Bond-orientational order in liquids and glasses. *Phys. Rev. B* 28:784–805
50. Mountain RD, Brown AC. 1984. Molecular dynamics investigation of homogeneous nucleation for inverse power potential liquids and for a modified Lennard-Jones liquid. *J. Chem. Phys.* 80:2730–34
51. Nosé S, Yonezawa F. 1986. Isothermal-isobaric computer simulations of melting and crystallization of a Lennard-Jones system. *J. Chem. Phys.* 84:1803–14
52. ten Wolde PR, Ruiz-Montero MJ, Frenkel D. 1995. Numerical evidence for bcc ordering at the surface of a critical fcc nucleus. *Phys. Rev. Lett.* 75:2714–17
53. Leyssale J-M, Delhommelle J, Millot C. 2003. A molecular dynamics study of homogeneous crystal nucleation in liquid nitrogen. *Chem. Phys. Lett.* 375:612–18
54. Leyssale J-M, Delhommelle J, Millot C. 2005. Atomistic simulation of the homogeneous nucleation and of the growth of N_2 crystallites. *J. Chem. Phys.* 122:104510
55. Desgranges C, Delhommelle J. 2007. Polymorph selection during the crystallization of Yukawa systems. *J. Chem. Phys.* 126:054501
56. Radhakrishnan R, Trout BL. 2002. A new approach for studying nucleation phenomena using molecular simulations: application to CO_2 hydrate clathrates. *J. Chem. Phys.* 117:1786–96

57. Leyssale J-M, Delhommelle J, Millot C. 2007. Hit and miss of classical nucleation theory as revealed by a molecular simulation study of crystal nucleation in supercooled sulfur hexafluoride. *J. Chem. Phys.* 127:044504
58. Valeriani C, Sanz E, Frenkel D. 2005. Rate of homogeneous crystal nucleation in molten NaCl. *J. Chem. Phys.* 122:194501
59. Ghiringhelli LM, Valeriani C, Los JH, Meijer EJ, Fasolino A, Frenkel D. 2008. State-of-the-art models for the phase diagram of carbon and diamond nucleation. *Mol. Phys.* 106:2011–38
60. Chau P-L, Hardwick AJ. 1998. A new order parameter for tetrahedral configurations. *Mol. Phys.* 93:511–18
61. Chaikin P, Lubensky T. 1995. *Principles of Condensed Matter Physics*. Cambridge/New York: Cambridge Univ. Press
62. Cuetos A, van Roij R, Dijkstra M. 2008. Isotropic-to-nematic nucleation in suspensions of colloidal rods. *Soft Matter* 4:757–67
63. Esselink K, Hilbers PAJ, van Beest BWH. 1994. Molecular dynamics study of nucleation and melting of *n*-alkanes. *J. Chem. Phys.* 101:9033–41
64. Yi P, Rutledge GC. 2009. Molecular simulation of crystal nucleation in *n*-octane melts. *J. Chem. Phys.* 131:134902
65. Beckham GT, Peters B, Trout BL. 2008. Evidence for a size dependent nucleation mechanism in solid state polymorph transformations. *J. Phys. Chem. B* 112:7460–66
66. Santiso EE, Trout BL. 2011. A general set of order parameters for molecular crystals. *J. Chem. Phys.* 134:064109
67. Shah M, Santiso EE, Trout BL. 2011. Computer simulations of homogeneous nucleation of benzene from the melt. *J. Phys. Chem. B* 115:10400–12
68. Heermann DW, Coniglio A, Klein W, Stauffer D. 1984. Nucleation and metastability in three-dimensional Ising models. *J. Stat. Phys.* 36:447–70
69. Wonczak S, Strey R, Stauffer D. 2000. Confirmation of classical nucleation theory by Monte Carlo simulations in the 3-dimensional Ising model at low temperature. *J. Chem. Phys.* 113:1976–80
70. Vehkamäki H, Ford IJ. 1999. Nucleation theorems applied to the Ising model. *Phys. Rev. E* 59:6483–88
71. Wedekind J, Reguera D. 2007. What is the best definition of a liquid cluster at the molecular scale? *J. Chem. Phys.* 127:154516
72. Vehkamäki H, Ford IJ. 2000. Critical cluster size and droplet nucleation rate from growth and decay simulations of Lennard-Jones clusters. *J. Chem. Phys.* 112:4193–202
73. Peters B, Trout BL. 2006. Obtaining reaction coordinates by likelihood maximization. *J. Chem. Phys.* 125:054108
74. Peters B. 2011. Recent advances in transition path sampling: accurate reaction coordinates, likelihood maximisation and diffusive barrier-crossing dynamics. *Mol. Simul.* 36:1265–81
75. Yang J-x, Gould H, Klein W. 1988. Molecular-dynamics investigation of deeply quenched liquids. *Phys. Rev. Lett.* 60:2665–68
76. Matsumoto M, Saito S, Ohmine I. 2002. Molecular dynamics simulation of the ice nucleation and growth process leading to water freezing. *Nature* 416:409–13
77. Torrie GM, Valleau JP. 1974. Monte Carlo free energy estimates using non-Boltzmann sampling: application to the sub-critical Lennard-Jones fluid. *Chem. Phys. Lett.* 28:578–81
78. Torrie GM, Valleau JP. 1977. Nonphysical sampling distributions in Monte Carlo free-energy estimation: umbrella sampling. *J. Comput. Phys.* 23:187–99
79. ten Wolde PR, Ruiz-Montero MJ, Frenkel D. 1996. Simulation of homogeneous crystal nucleation close to coexistence. *Faraday Discuss.* 104:93–110
80. Trudu F, Donadio D, Parrinello M. 2006. Freezing of a Lennard-Jones fluid: from nucleation to spinodal regime. *Phys. Rev. Lett.* 97:105701
81. Laio A, Gervasio FL. 2008. Metadynamics: a method to simulate rare events and reconstruct the free energy in biophysics, chemistry and material science. *Rep. Prog. Phys.* 71:126601
82. Plimpton S. 1995. Fast parallel algorithms for short-range molecular dynamics. *J. Comput. Phys.* 117:1–19
83. Berendsen HJC, van der Spoel D, van Drunen R. 1995. GROMACS: a message-passing parallel molecular dynamics implementation. *Comput. Phys. Commun.* 91:43–56

84. Binder K, Stauffer D. 1976. Statistical theory of nucleation, condensation and coagulation. *Adv. Phys.* 25:343–96
85. Stauffer D, Coniglio A, Heermann DW. 1982. Monte Carlo experiment for nucleation rate in the three-dimensional Ising model. *Phys. Rev. Lett.* 49:1299–302
86. Rikvold PA, Tomita H, Miyashita S, Sides SW. 1994. Metastable lifetimes in a kinetic Ising model: dependence on field and system size. *Phys. Rev. E* 49:5080–90
87. Berim GO, Ruckenstein E. 2002. Effect of shape on the critical nucleus size in a three-dimensional Ising model: energetic and kinetic approaches. *J. Chem. Phys.* 117:7732–37
88. Pan AC, Chandler D. 2004. Dynamics of nucleation in the Ising model. *J. Phys. Chem. B* 108:19681–86
89. Bartell LS, Wu DT. 2007. Do supercooled liquids freeze by spinodal decomposition? *J. Chem. Phys.* 127:174507
90. Peng LJ, Morris JR, Lo YC. 2008. Temperature-dependent mechanisms of homogeneous crystal nucleation in quenched Lennard-Jones liquids: molecular dynamics simulations. *Phys. Rev. B* 78:012201
91. Bhimalapuram P, Chakrabarty S, Bagchi B. 2007. Elucidating the mechanism of nucleation near the gas-liquid spinodal. *Phys. Rev. Lett.* 98:206104
92. Lundrigan SEM, Saika-Voivod I. 2009. Test of classical nucleation theory and mean first-passage time formalism on crystallization in the Lennard-Jones liquid. *J. Chem. Phys.* 131:104503
93. Wedekind J, Chkonia G, Wolk J, Strey R, Reguera D. 2009. Crossover from nucleation to spinodal decomposition in a condensing vapor. *J. Chem. Phys.* 131:114506
94. Bai X-M, Li M. 2006. Calculation of solid-liquid interfacial free energy: a classical nucleation theory based approach. *J. Chem. Phys.* 124:124707
95. Yi P, Rutledge GC. 2011. Molecular simulation of bundle-like crystal nucleation from *n*-eicosane melts. *J. Chem. Phys.* 135:024903
96. Bernstein J. 2002. *Polymorphism in Molecular Crystals*. Oxford/New York: Clarendon/Oxford Univ. Press
97. Bond AD. 2009. Polymorphism in molecular crystals. *Curr. Opin. Solid State Mater. Sci.* 13:91–97
98. Lee AY, Erdemir D, Myerson AS. 2011. Crystal polymorphism in chemical process development. *Annu. Rev. Chem. Biomol. Eng.* 2:259–80
99. Ostwald W. 1897. Studien über die Bildung und Umwandlung fester Körper. *Z. Phys. Chem.* 22:289–330
100. Klein W, Leyvraz F. 1986. Crystalline nucleation in deeply quenched liquids. *Phys. Rev. Lett.* 57:2845–48
101. Leyssale J-M, Delhommelle J, Millot C. 2004. Reorganization and growth of metastable α-N_2 critical nuclei into stable β-N_2 crystals. *J. Am. Chem. Soc.* 126:12286–87
102. Moroni D, ten Wolde PR, Bolhuis PG. 2005. Interplay between structure and size in a critical crystal nucleus. *Phys. Rev. Lett.* 94:235703
103. Desgranges C, Delhommelle J. 2006. Insights into the molecular mechanism underlying polymorph selection. *J. Am. Chem. Soc.* 128:15104–5
104. Sirota EB, Herhold AB. 1999. Transient phase-induced nucleation. *Science* 283:529–32
105. Rastogi S, Hikosaka M, Kawabata H, Keller A. 1991. Role of mobile phases in the crystallization of polyethylene. Part 1. Metastability and lateral growth. *Macromolecules* 24:6384–91
106. Magonov SN, Yerina NA, Ungar G, Reneker DH, Ivanov DA. 2003. Chain unfolding in single crystals of ultralong alkane $C_{390}H_{782}$ and polyethylene: an atomic force microscopy study. *Macromolecules* 36:5637–49
107. Muthukumar M. 2007. Shifting paradigms in polymer crystallization. In *Progress in Understanding of Polymer Crystallization*, ed. G Reiter, G Strobl, pp. 1–18. Berlin/Heidelberg: Springer
108. Cheng SZD. 2008. *Phase Transitions in Polymers: The Role of Metastable States*. Amsterdam/Boston: Elsevier
109. Swendsen RH, Wang J-S. 1986. Replica Monte Carlo simulation of spin-glasses. *Phys. Rev. Lett.* 57:2607–9
110. Carter EA, Ciccotti G, Hynes JT, Kapral R. 1989. Constrained reaction coordinate dynamics for the simulation of rare events. *Chem. Phys. Lett.* 156:472–77
111. West DK, Olmsted PD, Paci E. 2006. Free energy for protein folding from nonequilibrium simulations using the Jarzynski equality. *J. Chem. Phys.* 125:204910
112. Mu Y, Song X. 2006. Calculations of crystal-melt interfacial free energies by nonequilibrium work measurements. *J. Chem. Phys.* 124:034712

113. Hänggi P, Talkner P, Borkovec M. 1990. Reaction-rate theory: fifty years after Kramers. *Rev. Mod. Phys.* 62:251–341
114. ter Horst JH, Kashchiev D. 2003. Determination of the nucleus size from the growth probability of clusters. *J. Chem. Phys.* 119:2241–46
115. Bartell LS, Wu DT. 2006. A new procedure for analyzing the nucleation kinetics of freezing in computer simulation. *J. Chem. Phys.* 125:194503
116. Wedekind J, Strey R, Reguera D. 2007. New method to analyze simulations of activated processes. *J. Chem. Phys.* 126:134103
117. Kashchiev D. 2007. Interrelation between cluster formation time, cluster growth probability, and nucleation rate. *J. Chem. Phys.* 127:064505
118. Wedekind J, Reguera D. 2008. Kinetic reconstruction of the free-energy landscape. *J. Phys. Chem. B* 112:11060–63
119. Shaw DE, Maragakis P, Lindorff-Larsen K, Piana S, Dror RO, et al. Atomic-level characterization of the structural dynamics of proteins. *Science* 330:341–46
120. Chandler D. 1978. Statistical mechanics of isomerization dynamics in liquids and the transition state approximation. *J. Chem. Phys.* 68:2959–70
121. Bennett CH. 1977. Molecular dynamics and transition state theory: the simulation of infrequent events. In *Algorithms for Chemical Computations*, ed. RE Christophersen, pp. 63–97. Washington DC: Am. Chem. Soc.
122. Cichocki B, Hinsen K. 1990. Dynamic computer simulation of concentrated hard sphere suspensions: I. Simulation technique and mean square displacement data. *Phys. A: Stat. Mech. Appl.* 166:473–91
123. Bolhuis PG, Chandler D, Dellago C, Geissler PL. 2002. Transition path sampling: throwing ropes over rough mountain passes, in the dark. *Annu. Rev. Phys. Chem.* 53:291–318
124. Beckham GT, Peters B. 2010. New methods to find accurate reaction coordinates by path sampling. In *Computational Modeling in Lignocellulosic Biofuel Production*, ed. MR Nimlos, MF Crowley, pp. 299–332. Washington DC: Am. Chem. Soc.
125. van Erp TS, Moroni D, Bolhuis PG. 2003. A novel path sampling method for the calculation of rate constants. *J. Chem. Phys.* 118:7762–74
126. Moroni D, Bolhuis PG, van Erp TS. 2004. Rate constants for diffusive processes by partial path sampling. *J. Chem. Phys.* 120:4055–65
127. Moroni D, van Erp TS, Bolhuis PG. 2005. Simultaneous computation of free energies and kinetics of rare events. *Phys. Rev. E* 71:056709
128. Allen RJ, Valeriani C, ten Wolde PR. 2009. Forward flux sampling for rare event simulations. *J. Phys. Condens. Matter* 21:463102
129. Sanz E, Valeriani C, Frenkel D, Dijkstra M. 2007. Evidence for out-of-equilibrium crystal nucleation in suspensions of oppositely charged colloids. *Phys. Rev. Lett.* 99:055501
130. Vekilov PG. 2010. Nucleation. *Crystal Growth Des.* 10:5007–19

Annual Review of Chemical and Biomolecular Engineering

Volume 3, 2012

Contents

A Conversation with Haldor Topsøe
Haldor Topsøe and Manos Mavrikakis 1

Potential of Gold Nanoparticles for Oxidation in Fine Chemical Synthesis
Tamas Mallat and Alfons Baiker 11

Unraveling Reaction Pathways and Specifying Reaction Kinetics for Complex Systems
R. Vinu and Linda J. Broadbelt 29

Advances and New Directions in Crystallization Control
Zoltan K. Nagy and Richard D. Braatz 55

Nature Versus Nurture: Developing Enzymes That Function Under Extreme Conditions
Michael J. Liszka, Melinda E. Clark, Elizabeth Schneider, and Douglas S. Clark 77

Design of Nanomaterial Synthesis by Aerosol Processes
Beat Buesser and Sotiris E. Pratsinis 103

Single-Cell Analysis in Biotechnology, Systems Biology, and Biocatalysis
Frederik S.O. Fritzsch, Christian Dusny, Oliver Frick, and Andreas Schmid 129

Molecular Origins of Homogeneous Crystal Nucleation
Peng Yi and Gregory C. Rutledge 157

Green Chemistry, Biofuels, and Biorefinery
James H. Clark, Rafael Luque, and Avtar S. Matharu 183

Engineering Molecular Circuits Using Synthetic Biology in Mammalian Cells
Markus Wieland and Martin Fussenegger 209

Chemical Processing of Materials on Silicon: More Functionality, Smaller Features, and Larger Wafers
Nathan Marchack and Jane P. Chang 235

Engineering Aggregation-Resistant Antibodies
Joseph M. Perchiacca and Peter M. Tessier 263

Nanocrystals for Electronics
Matthew G. Panthani and Brian A. Korgel 287

Electrochemistry of Mixed Oxygen Ion and Electron Conducting Electrodes in Solid Electrolyte Cells
William C. Chueh and Sossina M. Haile 313

Experimental Methods for Phase Equilibria at High Pressures
Ralf Dohrn, José M.S. Fonseca, and Stephanie Peper 343

Density of States–Based Molecular Simulations
Sadanand Singh, Manan Chopra, and Juan J. de Pablo 369

Membrane Materials for Addressing Energy and Environmental Challenges
Enrico Drioli and Enrica Fontananova 395

Advances in Bioactive Hydrogels to Probe and Direct Cell Fate
Cole A. DeForest and Kristi S. Anseth 421

Materials for Rechargeable Lithium-Ion Batteries
Cary M. Hayner, Xin Zhao, and Harold H. Kung 445

Transport Phenomena in Chaotic Laminar Flows
Pavithra Sundararajan and Abraham D. Stroock 473

Sustainable Engineered Processes to Mitigate the Global Arsenic Crisis in Drinking Water: Challenges and Progress
Sudipta Sarkar, John E. Greenleaf, Anirban Gupta, Davin Uy, and Arup K. SenGupta 497

Complex Fluid-Fluid Interfaces: Rheology and Structure
Gerald G. Fuller and Jan Vermant 519

Atomically Dispersed Supported Metal Catalysts
Maria Flytzani-Stephanopoulos and Bruce C. Gates 521

Indexes

Cumulative Index of Contributing Authors, Volumes 1–3 575

Cumulative Index of Chapter Titles, Volumes 1–3 577

Errata

An online log of corrections to *Annual Review of Chemical and Biomolecular Engineering* articles may be found at http://chembioeng.annualreviews.org/errata.shtml